Magnetic properties of $Fe_{1-x}Ni_x$ alloy from CPA+DMFT perspectives

Alexander I. Poteryaev, Nikolay A. Skorikov, Vladimir I. Anisimov, and Michael A. Korotin
M. N. Miheev Institute of Metal Physics of Ural Branch of Russian Academy of Sciences, 18, S. Kovalevskaya Street, 620990 Ekaterinburg, Russia
(Received 30 October 2015; revised manuscript received 14 April 2016; published 18 May 2016)

We use a combination of the coherent potential approximation and dynamical mean field theory to study magnetic properties of the $Fe_{1-x}Ni_x$ alloy from first principles. Calculated uniform magnetic susceptibilities have a Curie-Weiss-like behavior, and extracted effective temperatures are in agreement with the experimental results. The individual squared magnetic moments obtained as a function of nickel concentration follow the same trends as experimental data. An analysis of the ionic and spin weights shows a possibility of high-spin to intermediate- and low-spin state transitions at high temperatures.

DOI: 10.1103/PhysRevB.93.205135

I. INTRODUCTION

Materials with transition metal elements are of great interest due to a large variety of physical properties: high-temperature superconductivity in copper and iron based compounds [1], giant magnetoresistance [2], metal-to-insulator transition [3], and many others. This diversity comes mainly from the fact that (i) the local Coulomb interaction of the 3*d* ions is comparable with its bandwidth and (ii) the *d* orbitals are partially filled. These compounds with competing kinetic and interacting energies can hardly be described by the conventional density functional theory (DFT) and are known as strongly correlated.

The elemental 3*d* metals with partially occupied shell are not exceptions. The famous 6 eV satellite in nickel [4] is of many body nature and cannot be described by a band structure theory [5]. An application of the state of the art DFT+DMFT method [6], that combines material specific aspects of the DFT and dynamical mean field theory [7] (DMFT) to treat correlated electrons, allowed to Lichtenstein *et al.* [8] describes properly electronic and magnetic properties of iron and nickel in ferro- and paramagnetic phases. Grechnev *et al.* [9], Di Marco *et al.* [10], Kolorenč *et al.* [11], and Minár *et al.* [12] studied spectral properties of Ni and found that correlation effects play an important role in forming satellite structure and renormalizing the exchange splitting. Benea *et al.* [13] calculated magnetic Compton profiles of Ni and Fe in DFT+DMFT approach and found that an inclusion of electronic correlations improves significantly an agreement between the theoretical and experimental results. Leonov *et al.*, in a series of papers [14–16], investigated a paramagnetic iron at ambient pressure as a function of temperature and found that a complete picture of phase transformations can be done when correlation effects are taken into account. Pourovskii *et al.* [17–19] studied magnetic and thermodynamic properties of iron at high pressure and concluded that correlations are important for phase stability.

In this view, an account for strong electron-electron interaction is required to investigate physical properties of $Fe_{1-x}Ni_x$ alloy, which was intensively studied due to the Invar effect discovered more than a hundred years ago [20]. One should note that a chemical disorder present in alloy complicates additionally a problem of a first principles description of materials. Nevertheless, different techniques to treat alloying effects are well developed in the framework of DFT. In one of the most used methods, a large supercell with randomly distributed atoms of different types is constructed, and then required properties can be evaluated from calculations for ordered structures. In a coherent potential approximation (CPA), a real crystal with randomly distributed ions is replaced by an effective medium with an energy-dependent self energy that has to be determined self-consistently (for recent reviews see [21] or [22] and references therein).

Magnetic properties of $Fe_{1-x}Ni_x$ alloy as a function of composition and volume were studied by several groups using both above mentioned approaches in the DFT framework. A rather complete review of these works can be found in a paper of Abrikosov *et al.* [23] who also found that a family of magnetic states are close to each other in energy and concluded that inclusion of strong electron-electron correlations is highly desired to reveal the physics of this alloy. Albeit the pure iron and nickel are successfully studied by means of DFT+DMFT method, there are only a few papers devoted to $Fe_{1-x}Ni_x$. Minár *et al.* [24,25] combined a Korringa-Kohn-Rostoker multiple scattering theory with the dynamical mean field theory and coherent potential approximation to treat substitutional disorder. For a solution of the effective impurity problem in DMFT they used fluctuation exchange approximation [26] in conjunction with T-matrix theory [27]. The authors found that a band broadening due to correlation effects and disorder is comparable in face centered cubic structure (fcc) of $Fe_{1-x}Ni_x$ below Curie temperature. Total magnetic moment is decreased as a function of Ni concentration. The individual magnetic moments for iron (nickel) are slightly overestimated (underestimated) [25] with respect to experimental values that can be connected to the perturbation nature of the impurity solver in DMFT. Vekilova *et al.* [28] investigated different phases of ordered $Fe_{0.75}Ni_{0.25}$ alloy at high pressure using DFT+DMFT method with continuous time quantum Monte Carlo as the impurity solver [29]. For a body centered cubic structure, a uniform magnetic susceptibility has a Curie-Weiss-like behavior, which changes to a Pauli type in a hexagonal close packed structure. They found that a strength of electronic correlations on the Fe 3*d* orbitals is sensitive to the phase and local environment.

In this paper, we study the magnetic properties of iron-rich fcc $Fe_{1-x}Ni_x$ binary alloy as a function of composition and temperature. To this aim, we utilize a combination of the coherent potential approximation with the dynamical mean field theory, which is described in the next section.

II. CPA+DMFT METHOD

The Hamiltonian of a crystal with a chemical type of disorder can be written as:

$$\hat{H} = \sum_{i\neq j}\sum_{m,m',\sigma} t^{\sigma}_{im,jm'}\hat{c}^{+}_{im\sigma}\hat{c}_{jm'\sigma} + \sum_{i,m,\sigma}\left(\epsilon^{i}_{m\sigma}-\mu\right)\hat{n}^{i}_{m\sigma} + \hat{H}_{\rm int}, \quad (1)$$

where $\hat{c}^{+}_{im\sigma}$ ($\hat{c}_{im\sigma}$) is a creation (annihilation) operator of an electron on site i with orbital m and spin σ. $\hat{n}^{i}_{m\sigma} = \hat{c}^{+}_{im\sigma}\hat{c}_{im\sigma}$. μ is a chemical potential, $t^{\sigma}_{im,jm'}$ are hopping amplitudes, $\epsilon^{i}_{m\sigma}$ is on-site energy. The last term in the Hamiltonian (1) corresponds to the on-site Coulomb interaction:

$$\hat{H}_{\rm int} = \frac{1}{2}\sum_{i,\{m\}}\sum_{\sigma\sigma'} U^{i}_{m'_1m'_2m_1m_2}\hat{c}^{+}_{m'_1\sigma}\hat{c}^{+}_{m'_2\sigma'}\hat{c}_{m_1\sigma'}\hat{c}_{m_2\sigma}, \quad (2)$$

where $U^{i}_{m'_1m'_2m_1m_2}$ are elements of the Coulomb interaction matrix. For the case of a substitutional disorder the on-site potential, $\epsilon^{i}_{m\sigma}$, and the Coulomb matrix, $U^{i}_{m'_1m'_2m_1m_2}$, depend on site index i, and they are different for different atomic species ϵ^{A}_{m} ($U^{A}_{m'_1m'_2m_1m_2}$) or ϵ^{B}_{m} ($U^{B}_{m'_1m'_2m_1m_2}$), depending on the atom remaining on site i with the probability x_A or x_B, $x_A + x_B = 1$. The hopping amplitudes are assumed to be site independent. This approximation seems reasonable for constituents with similar electronic structures, when the on-site local potentials are close in energy relative to their bandwidth [30–32].

The above Hubbard-type Hamiltonian (1) cannot be solved directly due to a simultaneous presence of the disorder and interaction. At the same time, the solutions of limiting cases, though approximate, are known. In the noninteracting limit, a coherent potential approximation [33] is utilized to describe the chemically disordered crystals. In the CPA, an electron propagation through the substitutionally disordered material is replaced by its propagation through an effective medium defined self-consistently. Another limiting case—absence of disorder (one type of atoms)—is known as the Hubbard model. One of the best single site approximations for its solution is the dynamical mean field theory [7,34]. In this theory the lattice problem is replaced by an effective impurity embedded in an energy dependent effective medium. The last has to be found self-consistently. Hence, both limiting cases at the hand share the effective medium or mean field interpretation of the problem.

To deal with the Hamiltonian (1) we will use the same effective medium ideology. Let us assume for the moment that the hybridization $\Delta(i\omega_n)$ of the embedded atom with the effective medium is known. Then, the local Green's functions are defined as

$$G_i = \frac{\int_0^{\beta}\hat{c}\hat{c}^{+}e^{-S_i}\mathcal{D}\hat{c}\mathcal{D}\hat{c}^{+}}{\int_0^{\beta}e^{-S_i}\mathcal{D}\hat{c}\mathcal{D}\hat{c}^{+}}, \quad (3)$$

where $\hat{c}$ and $\hat{c}^{+}$ are Grassman variables and an action is given as:

$$\begin{aligned} S_i = &-\sum_{nm\sigma}\hat{c}^{+}_{m\sigma}(i\omega_n)\left[\mu+i\omega_n-\epsilon^{i}_{m\sigma}-\Delta(i\omega_n)\right]\hat{c}_{m\sigma}(i\omega_n) \\ &+\frac{1}{2}\int_0^{\beta}d\tau\sum_{\{m\}}\sum_{\sigma\sigma'}U^{i}_{m'_1m'_2m_1m_2}\hat{c}^{+}_{m'_1\sigma}(\tau)\hat{c}^{+}_{m'_2\sigma'}(\tau) \\ &\times\hat{c}_{m_1\sigma'}(\tau)\hat{c}_{m_2\sigma}(\tau), \end{aligned} \quad (4)$$

where $\omega_n = (2n+1)\pi/\beta$ are the fermionic Matsubara frequencies, $\beta = 1/k_BT$ is an inverse temperature, and τ is an imaginary time. Self-consistency conditions require that the local Green's function should be equal to a weighted sum of impurity Green's functions:

$$G(i\omega_n) = x_A G_A(i\omega_n) + x_B G_B(i\omega_n). \quad (5)$$

Then, the local $G(i\omega_n)$ from Eq. (5) can be used to compute a self energy from the Dyson's equation:

$$\Sigma(i\omega_n) = i\omega_n - \Delta(i\omega_n) - G^{-1}(i\omega_n). \quad (6)$$

One should emphasize that the obtained self energy contains effects from the disorder and correlations simultaneously. This self energy is utilized to calculate the local Green's function of effective medium

$$G(i\omega_n) = \frac{1}{V_{\rm BZ}}\int_{BZ}\frac{d\mathbf{k}}{(\mu+i\omega_n)I - H(\mathbf{k}) - \Sigma(i\omega_n)}, \quad (7)$$

where $H(\mathbf{k})$ is the Fourier transform of the first term of the Hamiltonian (1) and an integration is performed over the first Brillouin zone with volume $V_{\rm BZ}$. The new hybridization function is then written as:

$$\Delta(i\omega_n) = i\omega_n - \Sigma(i\omega_n) - G^{-1}(i\omega_n). \quad (8)$$

The above set of equations are iteratively solved until a convergence with respect to the self energy or hybridization is achieved. One should note that the above described CPA+DMFT scheme behaves correctly in the different limits. Namely, if there is one type of atomic species all equations reduce to the conventional DMFT set. Another limit is noninteracting ($U^{\rm A}$=$U^{\rm B}$=0) and the equations become of classical CPA.

The generalization for a case of first principles calculations is straightforward. The DFT+DMFT Hamiltonian reads as

$$\hat{H}_{\rm DFT+DMFT} = \hat{H}_{\rm DFT} + \hat{H}_{\rm int} - \sum_{im\sigma}\varepsilon^{i}_{dc}\hat{n}^{i}_{m\sigma}, \quad (9)$$

where $\hat{H}_{\rm DFT}$ is the Hamiltonian in a localized basis set obtained within density functional theory framework. The second term is the interaction and it is described by Eq. (2). The density functional theory treats the Coulomb interaction in an averaged way, and therefore, one needs to subtract the so-called double counting term. The double counting is on-site quantity, and we use the fully localized limit in our calculations with the next definition for potential

$$\varepsilon^{i}_{dc} = \bar{U}^{i}\left(N^{i}_{d} - \frac{1}{2}\right), \quad (10)$$

where $\bar{U}^{i}$ is a mean Coulomb interaction and $N^{i}_{d} = \sum_{m\sigma} n^{i}_{m\sigma}$ is a total number of d electrons in DFT calculations.

The DFT+DMFT Hamiltonian (9) can be easily mapped to the disordered Hamiltonian (1). In such a case a matrix of hopping integrals in Eq. (1) become hoppings calculated in DFT, $t = t$(DFT), and the on-site energy is replaced as

$$\epsilon^{i}_{m\sigma} = \epsilon^{i}_{m\sigma}({\rm DFT}) - \varepsilon^{i}_{dc}, \quad (11)$$

where the right-hand part of the equation can be completely

defined within conventional band structure calculations.

III. RESULTS

For a first principles calculations, the Hamiltonian and related parameters [see Eq. (9)] were obtained using a full-potential linearized augmented-plane wave method implemented in the Exciting-plus code (a fork of ELK code [35]). The exchange-correlation potential was chosen in the Perdew-Burke-Ernzerhof form [36] of the generalized gradient approximation. The non-spin-polarized Hamiltonian $H(\mathbf{k})$ for fcc iron was constructed in a basis of well-localized Wannier functions [37] containing s, p, and d states. A reciprocal space was divided on the $18 \times 18 \times 18$ $\mathbf{k}$-points mesh in the full Brillouin zone. We utilized an experimental lattice constant [38], $a_{\mathrm{fcc}} = 3.5906$ Å, that corresponds to Invar alloy with the nickel concentration 35 at.%. To obtain on-site energies $\epsilon^i_{m\sigma}$, a supercell containing 15 Fe atoms and 1 Ni atom was constructed. The Hamiltonian of the supercell is then written in the Wannier function basis set, and the difference between iron and nickel on-site energies is defined as a difference between centers of gravity of corresponding d states, $\epsilon_d^{\mathrm{Fe}} - \epsilon_d^{\mathrm{Ni}} = \int (\rho_d^{\mathrm{Fe}}(\varepsilon) - \rho_d^{\mathrm{Ni}}(\varepsilon))\, \varepsilon\, d\varepsilon$, and it is equal to 0.88 eV [39]. This calculation was carried out for the nickel impurity in the iron host, hence, it is obvious that ϵ_d^{Fe}=0 eV and $\epsilon_d^{\mathrm{Ni}} = -0.88$ eV.

The CPA+DMFT calculations were performed with the AMULET code [40]. To solve an auxiliary impurity problem [Eq. (3)] arising in DMFT a segment version of the continuous time quantum Monte-Carlo (CT-QMC) method [29] was employed. This implementation of CT-QMC algorithm does not have a sign problem and it is faster than other quantum Monte-Carlo methods (for more details see review [41] and Ph.D. Thesis of E. Gull [42]). At the same time, it treats density-density terms of the Coulomb interaction in Eq. (2), neglecting spin-flips and pair-hopping contributions.

We used next values for the screened Coulomb interactions and Hund's exchange parameters, U^{Fe}=4 eV, U^{Ni}=6 eV, and J^{Fe}=J^{Ni}=0.9 eV. These values are in good agreement with results of constrained local density approximation calculations [43] and used in earlier DFT+DMFT papers for elemental iron [28,44]. Since the Coulomb interaction was already included in the density functional formalism, and thus in the Hamiltonian $H(\mathbf{k})$, we evaluate the double counting term according to Eq. (10). We used DFT values for the total number of d electrons, N_d^{Fe}=6.89 and N_d^{Ni}=8.77, that leads to a fixed values of double counting.

Inverse of uniform magnetic susceptibilities for various values of nickel concentrations are presented in Fig. 1. Keeping in mind a smaller value of Coulomb interaction and lattice constant in the paper of Vekilova *et al.* [28], the obtained results are in good qualitative agreement with the supercell DFT+DMFT data for $Fe_{0.75}Ni_{0.25}$. The uniform magnetic susceptibility was calculated in a linear response manner by applying a small external magnetic field B and evaluating magnetization of the compound $m(T)$ at a given temperature, $\chi(T) = m(T)/B$. One can clearly see that for all Ni concentrations χ^{-1} has a linear behavior at high temperatures that allows one to extract Curie-Weiss temperatures T_{CW} and effective magnetic moments μ^2_{eff} defined by the Curie-Weiss law,

$$\chi_{CW}(T) = \frac{\mu^2_{\mathrm{eff}}}{3(T - T_{CW})}.$$

The CPA+DMFT Curie-Weiss temperatures together with the experimental data [45–47] are shown in Fig. 2. The extracted T_{CW} follow very well its experimental counterparts. T_{CW} is risen with increasing of nickel concentrations, then it has a maximum around 65 at.% of Ni, and finally decreases at higher Ni percentage. In general, the theoretical Curie-Weiss temperatures are overestimated with respect to experimental values by factor, $T_{CW}^{\mathrm{Theor}}/T_{CW}^{\mathrm{Exp}} \approx 1.4$ (except for endpoints). This overestimation of the Curie-Weiss temperature is known in the DFT+DMFT calculations for various compounds [8,14,19,48] and it comes from two sources. The first source is a local nature of the DMFT approximation which leads to a $\mathbf{k}$-independent self-energy, and thus, neglecting

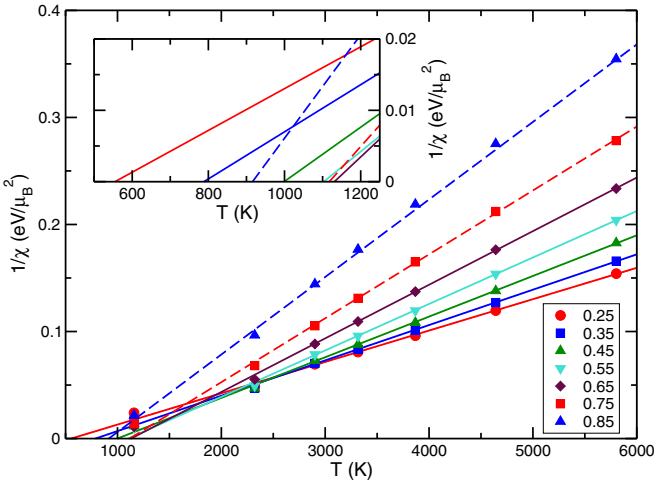

FIG. 1. Inverse of the uniform magnetic susceptibility, $\chi^{-1}(T)$, as a function of temperature for various values of nickel concentration in $Fe_{1-x}Ni_x$ (see color coding in figure). Inset shows scaled up region around the Curie-Weiss temperature T_{CW}.

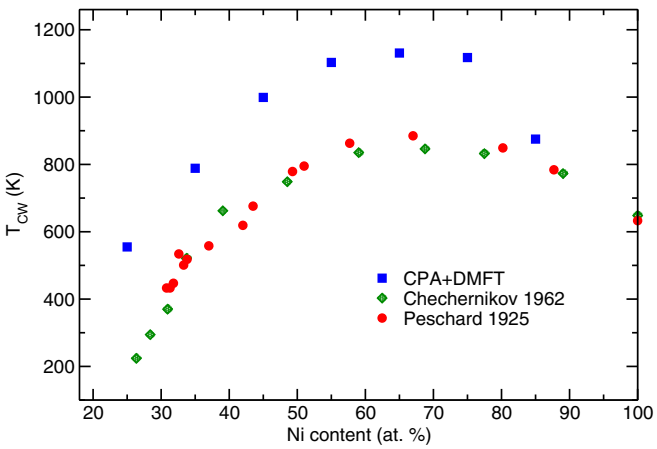

FIG. 2. CPA+DMFT and experimental values of Curie-Weiss temperature as a function of Ni concentration. Experimental data are from Chechernikov [45] and Peschard [46].

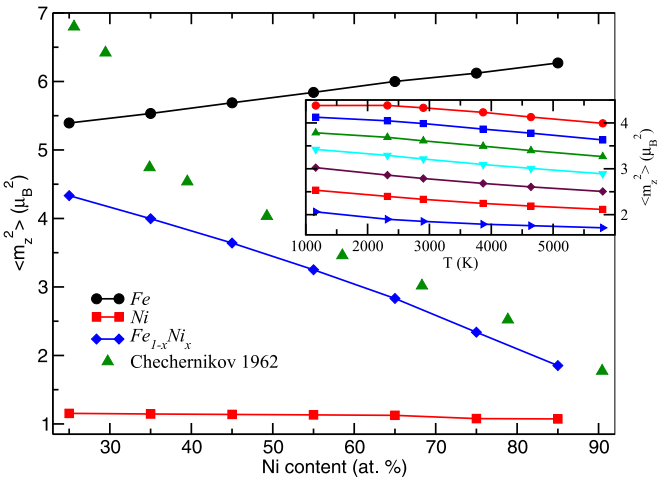

FIG. 3. Calculated at T=2900 K local squared magnetic moments, $\langle m_z^2 \rangle$, for Fe, Ni and $Fe_{1-x}Ni_x$ alloy as a function of Ni concentration (for color coding see figure). Experimental effective magnetic moments extracted from paramagnetic susceptibility [45] are shown by green triangles. Inset shows a temperature dependence of alloys $\langle m_z^2 \rangle$ for various nickel concentrations (color coding is the same as in Fig. 1).

spacial correlation effects that are important in a vicinity of the magnetic transition. Since the lattice is fixed the effect of neglecting spacial long range correlations on the uniform susceptibility is approximately the same for various alloy concentrations. The second reason of overestimation originates from a density-density form of the Coulomb interaction in a segment version of CT-QMC algorithm [49,50]. The better agreement for the Curie temperature at high nickel content is attributed with lesser importance of spin-flip and pair hopping terms in an almost filled d shell [51]. Therefore, keeping in mind the above mentioned arguments, the theoretical CPA+DMFT Curie-Weiss temperatures agree very well with the experimental data and, what is more important, they are changed with nickel content in exactly the same way as in experiment.

Local squared magnetic moments for iron, nickel, and their weighted sum are presented in Fig. 3. The local squared magnetic moment is defined as

$$\langle m_z^2 \rangle^i = \left\langle \sum_{mm'} \left(\hat{n}^i_{m\uparrow} - \hat{n}^i_{m\downarrow}\right)\left(\hat{n}^i_{m'\uparrow} - \hat{n}^i_{m'\downarrow}\right) \right\rangle,$$

where i=(Fe,Ni) and the corresponding quantity for the alloy is $\langle m_z^2 \rangle = (1-x)\langle m_z^2 \rangle^{\mathrm{Fe}} + x\langle m_z^2 \rangle^{\mathrm{Ni}}$. Local squared magnetic moment of nickel is slowly decreasing with Ni concentration from 1.15 to 1.07 while iron's function is almost linearly increasing with values from 5.39 to 6.27. The resulting alloy's $\langle m_z^2 \rangle$ is quadratically decreasing and it follows the experimental effective magnetic moments extracted from paramagnetic susceptibility [45]. The large discrepancy is observed at nickel concentrations below 30 at.%, and it is attributed to the experimentally observed coexistence of face centered cubic and body centered cubic phase [52] not presented in the calculations. In spite of the fact that the local magnetic moments were calculated in paramagnetic phase, their concentration behavior corresponds to the atomically resolved experimental data [53–55] obtained for the magnetically ordered alloys and

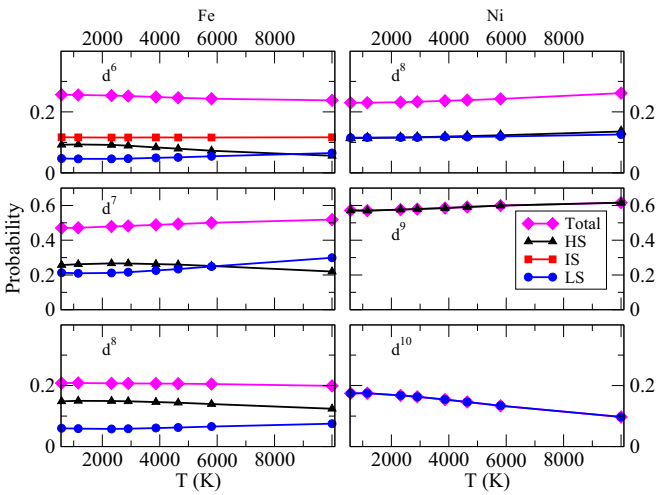

FIG. 4. Probabilities of different ionic configurations and spin states for Fe and Ni in $Fe_{0.75}Ni_{0.25}$ alloys as function of temperature. Weight of the ionic configuration (total) is shown by magenta diamonds, while high- (HS), intermediate- (IS) and low- (LS) spin states are presented by black triangles, red squares and blue circles, respectively.

to the earlier DFT+DMFT results [24]. Inset of Fig. 3 shows a temperature dependence of the local squared magnetic moment of $Fe_{1-x}Ni_x$ alloy in the concentration range x=[0.25...0.85]. For all studied concentrations it is decreased with temperature as in a pure fcc-Fe [19].

To analyze in more details a temperature and concentration dependence of the magnetic properties of constituents in $Fe_{1-x}Ni_x$ we present distributions of ionic weights and corresponding spin configurations in Figs. 4–7. In the right panel of these figures the d^8, d^9, and d^{10} ionic configurations of nickel are shown by magenta diamonds. For all temperature and concentration ranges the high-spin ($d^{5\uparrow}d^{4\downarrow}$) state of d^9 ionic configuration has the largest weight like in the pure nickel [11]. The weight of d^8 contribution is much smaller and it is equally distributed between high-spin ($d^{5\uparrow}d^{3\downarrow}$) and

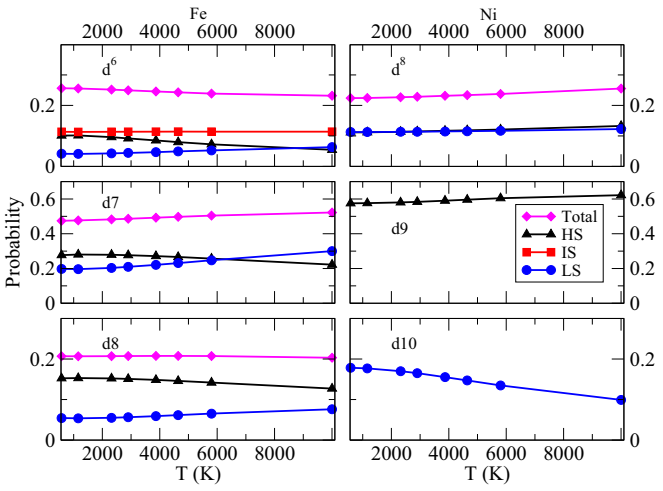

FIG. 5. Probabilities of different ionic configurations and spin states for Fe and Ni in $Fe_{0.65}Ni_{0.35}$ alloys as function of temperature. Color-coding as in Fig. 4.

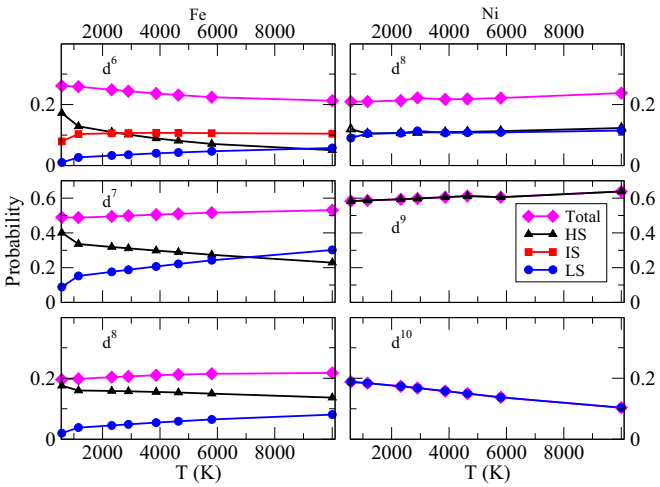

FIG. 6. Probabilities of different ionic configurations and spin states for Fe and Ni in $Fe_{0.35}Ni_{0.65}$ alloys as function of temperature. Color coding as in Fig. 4.

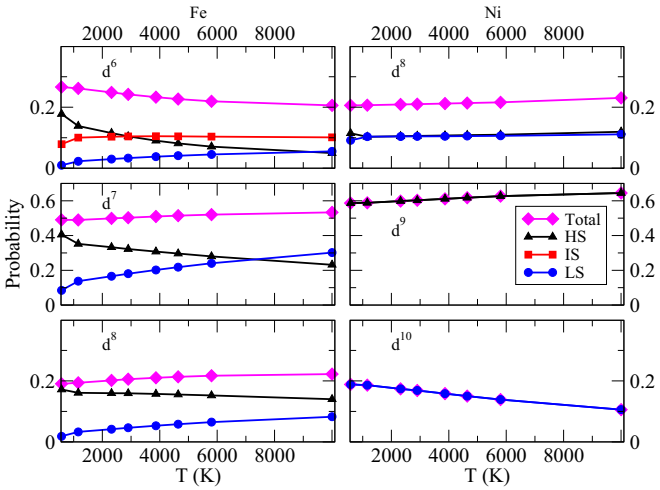

FIG. 7. Probabilities of different ionic configurations and spin states for Fe and Ni in $Fe_{0.25}Ni_{0.75}$ alloys as function of temperature. Color-coding as in Fig. 4.

low-spin ($d^{4\uparrow}d^{4\downarrow}$) states. The d^8 and d^9 contributions are monotonically increasing with temperature. The low-spin state of d^{10} configuration is even smaller and it is decreasing with temperature. All these states are almost independent of nickel percentage in $Fe_{1-x}Ni_x$ and sum of the d^8 and d^{10} total weights is about two times smaller than weight of d^9 ionic state. At the same time, the occupation of d manifold in nickel is almost independent of temperature and concentration in all CPA+DMFT calculations and it equals to 8.9 ± 0.07 electrons, which is comparable with the DFT value of 8.77.

The situation with the states of iron presented in the left panel of Figs. 4–7 is more interesting. The major contribution is formed by the d^7 ionic state but now satellite's total weights are comparable and the sum of d^6 and d^8 ionic weights is approximately of d^7 weight. For the d^8 ionic configuration the weight of the low-spin ($d^{4\uparrow}d^{4\downarrow}$) state is smaller than the weight of high-spin ($d^{5\uparrow}d^{3\downarrow}$). The later is decreasing with temperature while the former is increasing but they are not crossed in the temperature range of investigation. This qualitative behavior of low- and high-spin states is kept for all nickel concentrations. In the case of d^7 ionic configuration the weight of the high-spin ($d^{5\uparrow}d^{2\downarrow}$) state is increasing with the temperature, while the low-spin ($d^{4\uparrow}d^{3\downarrow}$) state is decreasing and these spin configurations are intersecting around 6000 K with a shift to higher temperatures at nickel-rich alloy.

The situation with the d^6 ionic configuration is even more complicated because an intermediate-spin ($d^{4\uparrow}d^{2\downarrow}$) state can be realized besides the high- ($d^{5\uparrow}d^{1\downarrow}$) and low-spin ($d^{3\uparrow}d^{3\downarrow}$). Exactly this intermediate-spin state dominates at high temperatures for all nickel concentrations and it let the high-spin state be major at ≈ 50 at.% and low temperatures. Thus, in the iron-rich $Fe_{1-x}Ni_x$ (see Figs. 4 and 5) the high-spin state has more weight for $T < 2900$ K. In fact, in the d^6 ionic state there are two points of spin state alternations. At high temperatures the intermediate-spin is a major, the high-spin is a minor and the low-spin state is in between. At $T \approx 7300$ K the high-spin and the low-spin states are switched and then at $T \approx 2900$ K and for nickel concentrations $x > 0.45$ the high-spin and the intermediate-spin states are interchanged. The $3d$ Fe occupation is almost independent of temperature and concentration (like for nickel) and it equals to 6.93 ± 0.06 electrons, which is a bit higher than the DFT value of 6.89.

Albeit these spin state transitions in iron occur at the temperatures much above the experimental Curie-Weiss one (keeping in mind that $T_{CW}^{\text{Theor}} = 1.4T_{CW}^{\text{Exp}}$), a high temperature local atomic physics of paramagnetic system can be traced back to the magnetically ordered phase. Thus these transitions can be regarded as a realization of two possible electronic states in γ-Fe with the ferromagnetic high volume and the antiferromagnetic low volume states proposed by Weiss [56]. One can also think of this rich local physics as of a variety of magnetically ordered phases at low temperatures found in the conventional DFT calculations as function of volume (see Ref. [23] and references therein).

IV. CONCLUSION

We formulated and implemented in computer codes the CPA+DMFT method which combines a coherent potential approximation and dynamical mean field theory in one technique and treats a substitutional disorder and strong electron-electron correlations on equal footing. Then this CPA+DMFT method were applied to study the magnetic properties of $Fe_{1-x}Ni_x$ alloy above the Curie temperature. The calculated inverse of the uniform magnetic susceptibilities show a linear behavior at high temperatures and extracted Curie-Weiss temperatures follow the experimental values as function of nickel concentration. The individual local squared magnetic moments for iron and nickel are in good agreement with experimental data. The analysis of the contributions to the ionic and spin configurations shows the alternating of the high-spin state and, intermediate- and low-spin states, as function of temperature that is in agreement with the two state theory of Weiss [56]. These transitions can be regarded as a

high temperature precursor of a multiple magnetic orders at low temperatures found in the density functional calculations. Since they are strongly overestimated the further CPA+DMFT studies for different volumes and interaction parameters are of great interests.

ACKNOWLEDGMENTS

The authors are grateful to Yu. N. Gornostyrev, A. S. Belozerov, and S. L. Skornyakov for useful discussions. The study was supported by the Russian Scientific Foundation through the project 14-12-00473.

[1] G. R. Stewart, Rev. Mod. Phys. **83**, 1589 (2011)
[2] A. Fert, Rev. Mod. Phys. **80**, 1517 (2008).
[3] M. Imada, A. Fujimori, and Y. Tokura, Rev. Mod. Phys. **70**, 1039 (1998).
[4] C. Guillot, Y. Ballu, J. Paigné, J. Lecante, K. P. Jain, P. Thiry, R. Pinchaux, Y. Pétroff, and L. M. Falicov, Phys. Rev. Lett. **39**, 1632 (1977).
[5] R. Clauberg, W. Gudat, E. Kisker, E. Kuhlmann, and G. M. Rothberg, Phys. Rev. Lett. **47**, 1314 (1981).
[6] V. I. Anisimov, A. I. Poteryaev, M. A. Korotin, A. O. Anokhin, and G. Kotliar, J. Phys.: Condens. Matter **9**, 7359 (1997); A. I. Lichtenstein and M. I. Katsnelson, Phys. Rev. B **57**, 6884 (1998).
[7] A. Georges, G. Kotliar, W. Krauth, and M. J. Rozenberg, Rev. Mod. Phys. **68**, 13 (1996).
[8] A. I. Lichtenstein, M. I. Katsnelson, and G. Kotliar, Phys. Rev. Lett. **87**, 067205 (2001).
[9] A. Grechnev, I. Di Marco, M. Katsnelson, A. Lichtenstein, J. Wills, and O. Eriksson, Phys. Rev. B **76**, 035107 (2007).
[10] I. Di Marco, J. Minár, S. Chadov, M. I. Katsnelson, H. Ebert, and A. I. Lichtenstein, Phys. Rev. B **79**, 115111 (2009).
[11] J. Kolorenč, A. I. Poteryaev, and A. I. Lichtenstein, Phys. Rev. B **85**, 235136 (2012).
[12] J. Minár, J. Braun, and H. Ebert, J. Electron Spectrosc. Relat. Phenom. **189**, 129 (2013).
[13] D. Benea, J. Minár, L. Chioncel, S. Mankovsky, and H. Ebert, Phys. Rev. B **85**, 085109 (2012).
[14] I. Leonov, A. I. Poteryaev, V. I. Anisimov, and D. Vollhardt, Phys. Rev. Lett. **106**, 106405 (2011).
[15] I. Leonov, A. I. Poteryaev, V. I. Anisimov, and D. Vollhardt, Phys. Rev. B **85**, 020401 (2012).
[16] I. Leonov, A. I. Poteryaev, Y. N. Gornostyrev, A. I. Lichtenstein, M. I. Katsnelson, V. I. Anisimov, and D. Vollhardt, Sci. Rep. **4**, 5585 (2014).
[17] L. V. Pourovskii, T. Miyake, S. I. Simak, A. V. Ruban, L. Dubrovinsky, and I. A. Abrikosov, Phys. Rev. B **87**, 115130 (2013).
[18] L. V. Pourovskii, J. Mravlje, M. Ferrero, O. Parcollet, and I. A. Abrikosov, Phys. Rev. B **90**, 155120 (2014).
[19] P. A. Igoshev, A. V. Efremov, A. I. Poteryaev, A. A. Katanin, and V. I. Anisimov, Phys. Rev. B **88**, 155120 (2013).
[20] C. E. Guillaume and C. R. Hebd, Seances Acad. Sci. **125**, 235 (1897).
[21] A. V. Ruban and I. A. Abrikosov, Rep. Prog. Phys. **71**, 046501 (2008).
[22] D. A. Rowlands, Rep. Prog. Phys. **72**, 086501 (2009).
[23] I. A. Abrikosov, A. E. Kissavos, F. Liot, B. Alling, S. I. Simak, O. Peil, and A. V. Ruban, Phys. Rev. B **76**, 014434 (2007).
[24] J. Minár, L. Chioncel, A. Perlov, H. Ebert, M. I. Katsnelson, and A. I. Lichtenstein, Phys. Rev. B **72**, 045125 (2005).
[25] J. Minár, S. Mankovsky, O. Šipr, D. Benea, and H. Ebert, J. Phys.: Condens. Matter **26**, 274206 (2014).
[26] N. E. Bickers and D. J. Scalapino, Ann. Phys. **193**, 206 (1989).
[27] V. M. Galitski, JETP **7**, 104 (1958); **7**, 698 (1958); J. Kanamori, Prog. Theor. Phys. **30**, 275 (1963).
[28] O. Yu. Vekilova, L. V. Pourovskii, I. A. Abrikosov, and S. I. Simak, Phys. Rev. B **91**, 245116 (2015).
[29] P. Werner, A. Comanac, L. de'Medici, M. Troyer, and A. J. Millis, Phys. Rev. Lett. **97**, 076405 (2006).
[30] J. S. Faulkner, Prog. Mater. Sci. **27**, 1 (1982).
[31] F. Ducastelle, *Order and Phase Stability in Alloys* (North-Holland, Amsterdam, 1991).
[32] I. A. Abrikosov and B. Johansson, Phys. Rev. B **57**, 14164 (1998).
[33] P. Soven, Phys. Rev. **156**, 809 (1967).
[34] W. Metzner and D. Vollhardt, Phys. Rev. Lett. **62**, 324 (1989); G. Kotliar and D. Vollhardt, Phys. Today **57**, 53 (2004).
[35] http://elk.sourceforge.net/.
[36] J. P. Perdew, K. Burke, and M. Ernzerhof, Phys. Rev. Lett. **77**, 3865 (1996).
[37] Dm. Korotin, A. V. Kozhevnikov, S. L. Skornyakov, I. Leonov, N. Binggeli, V. I. Anisimov, and G. Trimarchi, Eur. Phys. J. B **65**, 91 (2008).
[38] R. P. Reed and R. E. Schramm, J. Appl. Phys. **40**, 3453 (1969).
[39] Calculations for the 25 at.% of nickel give the value of the on-site splitting between Fe and Ni equal to 0.97 eV which modifies slightly numerics and does not change the main results qualitatively.
[40] http://www.amulet-code.org/.
[41] E. Gull, A. J. Millis, A. I. Lichtenstein, A. N. Rubtsov, M. Troyer, and P. Werner, Rev. Mod. Phys. **83**, 349 (2011).
[42] E. Gull, Ph.D. thesis, ETH Zurich, 2008.
[43] F. Aryasetiawan, K. Karlsson, O. Jepsen, and U. Schonberger, Phys. Rev. B **74**, 125106 (2006).
[44] A. S. Belozerov and V. I. Anisimov, J. Phys.: Condens. Matter **26**, 375601 (2014).
[45] V. I. Chechernikov, JETP **15**, 659 (1962).
[46] M. Peschard, Rev. Metall. **22**, 430 (1925).
[47] L. J. Swartzendruber, V. P. Itkin, and C. B. Alcock, J. Phase Equilib. **12**, 288 (1991).
[48] A. S. Belozerov, A. I. Poteryaev, and V. I. Anisimov, JETP Lett. **93**, 70 (2011).
[49] Shiro Sakai, Ryotaro Arita, Karsten Held, and Hideo Aoki, Phys. Rev. B **74**, 155102 (2006).

[50] V. I. Anisimov, A. S. Belozerov, A. I. Poteryaev, and I. Leonov, Phys. Rev. B **86**, 035152 (2012).
[51] A. E. Antipov, I. S. Krivenko, V. I. Anisimov, A. I. Lichtenstein, and A. N. Rubtsov, Phys. Rev. B **90**, 039909(E) (2014).
[52] L. McKeehan, Phys. Rev. **21**, 402 (1923).
[53] C. G. Shull and M. K. Wilkinson, Phys. Rev. **97**, 304 (1955).
[54] J. W. Cable and E. O. Wollan, Phys. Rev. B **7**, 2005 (1973).
[55] B. Glaubitz, S. Buschhorn, F. Brüssing, R. Abrudan, and H. Zabel, J. Phys.: Condens. Matter **23**, 254210 (2011).
[56] R. J. Weiss, Proc. Phys. Soc. **82**, 281 (1963).